Absolute two-photon absorption coefficients at 355 and 266 nm

P. Liu, W. L. Smith,* H. Lotem, J. H. Bechtel,† and N. Bloembergen
Gordon McKay Laboratory, Harvard University, Cambridge, Massachusetts 02138

R. S. Adhav
Quantum Technology Inc., Grand Island, New York 14072
(Received 10 November 1977)

The absolute two-photon absorption coefficients of uv-transmitting materials have been measured using well-calibrated single picosecond pulses, at the third and fourth harmonic of a mode-locked YAlG:Nd laser system. Two-photon abosorption coefficients of the order of 10^{-3} cm/MW were measured for alkali halides, and 10^{-4} cm/MW for harmonic-generating crystals. In materials with band gap greater than $2\hbar\omega$, no nonlinear absorption could be observed. Calculations based on the Keldysh theory with one adjustable parameter agree quite well with the experimentally observed dispersions in the two-photon absorption coefficients. The effect of multiphoton absorption on the conversion efficiency of harmonic generating crystals and on the breakdown of uv window materials is also discussed.

I. INTRODUCTION

The first theoretical study on two-photon absorption (TPA) processes was carried out by Goppert-Mayer[1] in 1931. With the advent of the ruby lasers, Kaiser and Garrett[2] observed TPA at optical frequencies in 1961. Several techniques have subsequently been used to find TPA coefficients, for example, by measuring the intensity-dependent transmission through two-photon excitation. Several comprehensive reviews of TPA are available.[3-5]

Absolute TPA coefficients can only be obtained directly by well-calibrated lasers. However, relative measurements can be done quite simply by the two-channel technique.[6] The same technique may also be used to obtain absolute TPA coefficients by utilizing known Raman cross sections.[7] Since the TPA coefficient is related to the imaginary part of the third-order nonlinear susceptibility, parametric mixing experiments such as three-wave mixing which are capable of measuring the real and imaginary part of the third-order nonlinear susceptibility have been used to find TPA cross sections.[8]

TPA studies have both scientific and technological interest. Because the TPA selection rules are different in general from the linear spectroscopy selection rules, TPA data may provide new information about electronic wave functions and energy levels in the material. In particular, additional information on band structure in solids may be obtained. Practically, the TPA process has been used to excite bulk carriers in large semiconductor crystals and generate color centers in some alkali halides. These effects have been used for pumping semiconductor lasers[9] and distributed-feedback tunable ir lasers.[10] The multiphoton absorption provides a damage mechanism,[11,12] and thus it may determine the damage threshold of the material. This mechanism is especially important in uv windows. With the recent development in high-power uv lasers, practical interest has arisen in the absolute TPA coefficients of the window materials in the uv region where published data are quite limited. In harmonic-generating crystals, the limited conversion efficiencies have been assigned to nonlinear absorption,[13] or to phase mismatch[14] by different authors. Accurate measurement of the nonlinear absorption coefficients is useful in resolving this issue.

In Sec. II, a brief review of pertinent theories of TPA in solids is presented. The experimental setup and procedure are discussed in Sec. III. In Sec. IV, the results are presented and in Sec. V, our results are compared with calculations based on the Keldysh theory of high-frequency tunneling.

II. THEORY

In materials with band gap greater than one photon but smaller than the two-photon energy of an interacting light, it is possible to have absorption by simultaneously absorbing two or more photons from a single laser beam. The two-photon transition rate per unit volume may be obtained by the second-order perturbation theory

$$W^{(2)}=\frac{(2\pi)^3}{n_0^2c^2\hbar^2}\left(\frac{I}{\hbar}\right)^2\sum_f |M_{fg}|^2\delta(\omega_{fg}-2\omega)\,, \qquad (1)$$

where

$$M_{fg}=\frac{e^2}{m^2\omega^2}\sum_i \frac{(\vec{p}_{fi}\cdot\hat{a})(\vec{p}_{ig}\cdot\hat{a})}{\omega_{ig}-\omega}\,,$$

n_0 is the index of refraction, c is the velocity of light in vacuum, m and e are the mass and charge of the electron, respectively, and I is the intensity of the laser. Summations are extended over final states $|f\rangle$ and intermediate states $|i\rangle$. The initial ground state is denoted by $|g\rangle$. $\hat{a}$ is a unit vector in the direction of the electric field. $\vec{p}_{ij}$ is the matrix element of the momentum operator between the states i and j. $\hbar\omega_{ij}$ is the energy difference between the latter states.

In the standard perturbation approach, the matrix elements and the energy levels [see Eq. (1)] are found from the solutions of the unperturbed Hamiltonian. Another approach to attack the high-order transition-rates problem was developed by Keldysh,[15] who takes into account the main effect of the electromagnetic field at the first step of the calculations. In this formalism, the transition rate between the Stark-shifted states

$$\psi(\vec{r},t)=U_{\vec{p}(t)}(\vec{r}) \times \exp\left[\frac{i}{\hbar}\left(\vec{p}(t)\cdot\vec{r}-\int_0^t \mathcal{E}(\vec{p}(\tau))\,d\tau\right)\right], \quad (2)$$

where

$$\vec{p}(t)=\vec{p}+(e\vec{E}/\omega)\sin\omega t$$

is obtained. This approach is useful since it takes into account all orders of the perturbation expansion. Using this technique, the multiphoton ionization rate in both gases and solids had been calculated by Keldysh[15] and others.[16] Keldysh's expression for the transition rate reduces to tunneling at low frequencies while at high frequencies the result reduces to multiphoton absorption. In a solid with fundamental energy-band gap E_g, using a simple parabolic energy-band structure,[15] the multiphoton transition rate per unit volume is given by the Keldysh formula

$$W=\frac{2}{9\pi}\omega\left(\frac{m^*\omega}{\hbar}\right)^{3/2}\Phi\left[\left(2\left\langle\frac{\Delta}{\hbar\omega}+1\right\rangle-2\frac{\Delta}{\hbar\omega}\right)^{1/2}\right] \times \exp\left[2\left\langle\frac{\Delta}{\hbar\omega}+1\right\rangle\left(1-\frac{e^2E^2}{4m^*\omega^2E_g}\right)\right] \times\left(\frac{e^2E^2}{16m^*\omega^2E_g}\right)^{\langle\Delta/\hbar\omega+1\rangle}, \quad (3)$$

where

$$\Delta=E_g+e^2E^2/4m^*\omega^2.$$

$\Phi(z)=e^{-z^2}\int_0^z e^{y^2}\,dy$ is the Dawson integral. E is the peak field, m^* is the effective reduced mass of the electron and hole pair, $\langle\ \rangle$ denotes the integer part of the argument.

The complex field dependence of this equation may be simplified in the high-frequency limit. The dominant field dependence is then given by the last factor in the transition rate [Eq. (3)]. The N-photon absorption coefficient γ_N is defined by the expression

$$\gamma_N=\frac{2}{9\pi}N\hbar\omega^2\left(\frac{8\pi}{n_0}\right)^N\left(\frac{m^*\omega}{\hbar}\right)^{3/2}\Phi\left[\left(2N-2\frac{\Delta}{\hbar\omega}\right)^{1/2}\right] \times\exp\left[2N\left(1-\frac{e^2E^2}{4m^*\omega^2E_g}\right)\right]\left(\frac{e^2}{16m^*\omega^2E_g}\right)^N, \quad (4)$$

which has only a very weak field dependence through Δ. The cross sections may be obtained by transmission versus laser-intensity measurements. In the case of one- and two-photon absorbing media one obtains, with $\gamma_1=\alpha$ and $\gamma_2=\beta$, for the transmitted intensity

$$I(\vec{r},l,t)=\frac{(1-R)^2I(\vec{r},0,t)e^{-\alpha l}}{1+\beta(1-R)I(\vec{r},0,t)(1-e^{-\alpha l})/\alpha}, \quad (5)$$

where l is the length of the sample, and R is the reflectivity.[17] Multiple reflections are neglected in the derivation of the above equation.

Since we wish to compare in this paper multiphoton transitions of different order, we have used the Keldysh theory for estimations of multiphoton cross sections. Because this theory is based on a very simplified band structure, the present calculations are not expected to be accurate. Satisfactory agreement, however, was achieved between the dispersion of β measured here and the Keldysh expression, using one adjustable parameter.

The TPA coefficient may also be expressed in terms of the imaginary part of the third-order nonlinear susceptibility tensor $\chi^{(3)}_{ijkl}(-\omega,\omega,\omega,-\omega)$. For cubic crystals, with 432, $\bar{4}3m$, or $m3m$ symmetry and a single laser frequency, $\chi^{(3)}$ has only three independent elements.[18] These elements may be obtained by the measurement of the TPA cross section in three different polarization conditions. First, it is convenient to measure the diagonal element χ''_{xxxx} according to the relation

$$\beta=(32\pi^2\omega/n_0^2c^2)[3\chi''_{xxxx}(-\omega,\omega,\omega,-\omega)], \quad (6)$$

which is derived in Appendix A. Here ω is the laser angular frequency, c is the speed of light in vacuum, and n_0 is the index of refraction. We are using the Maker and Terhune convention,[19] with a degeneracy factor of 3, because there are three distinct permutations of the positive and negative frequency arguments. As shown in Appendix A, for linearly polarized light in the [110] direction, the TPA coefficient is

$$\beta=(16\pi^2\omega/n_0^2c^2)[3\chi''_{xxxx}(-\omega,\omega,\omega,-\omega) + 6\chi''_{xxyy}(-\omega,\omega,\omega,-\omega) + 3\chi''_{xyyx}(-\omega,\omega,\omega,-\omega)], \quad (7)$$

and for circularly polarized light, with light propagating along [001], it is

$$\beta = (16\pi^2\omega/n_0^2c^2)[3\chi''_{xxxx}(-\omega,\omega,\omega,-\omega) + 6\chi''_{xxyy}(-\omega,\omega,\omega,-\omega) - 3\chi''_{xyyx}(-\omega,\omega,\omega,-\omega)]. \quad (8)$$

III. EXPERIMENTAL SETUP AND PROCEDURE

The YAlG:Nd laser oscillator-amplifier system is described in Ref. 17. Passive mode locking is employed with a spark-triggered electro-optical shutter to select a single pulse having energy up to 10 mJ. The beam profile was measured carefully. It is Gaussian both in space and time. The pulses have an average duration of 30 psec at full width at half maximum. The fundamental laser frequency is doubled by a temperature-tuned 90° phase-matched cesium dihydrogen arsenate (CDA) crystal [see Fig. 1(a)]. The energy conversion efficiency at 100-MW input is 50%. The third harmonic (355 nm) is generated by mixing the fundamental and the second-harmonic frequencies in an angle tuned potassium dihydrogen phosphate (KDP) crystal. The energy profile of the beam is monitored by photodiode array R, and fitted with a Gaussian curve with a $1/e$ radius $d = 0.78$ mm. The fourth harmonic (266 nm) is generated by frequency doubling the second harmonic in a temperature-tuned 90° phase-matched ammonium dihydrogen phosphate (ADP) crystal. The beam is again fitted with a Gaussian of radius $d = 0.68$ mm. The overall energy-conversion efficiency to 355 nm is 10%; to 266 nm it is 15%. Unwanted frequencies are filtered out by color filters as shown in Fig. 1(a), or by a dispersive prism used at minimum deviation in order not to distort the beam.

In order to determine the TPA cross section, the energy-transmission coefficient through the sample is measured. For a Gaussian beam with a maximum on-axis input intensity I_p, we may write for the transmitted intensity

$$I(r,l,t) = \frac{I_p(1-R)^2 \exp[-(r/d)^2 - (t/\tau)^2]e^{-\alpha l}}{1+\beta I_p(1-R)\exp[-(r/d)^2-(t/\tau)^2](1-e^{-\alpha l})}, \quad (9)$$

while the energy transmission coefficient is given by

$$T = \frac{\mathcal{E}^{\text{out}}}{\mathcal{E}^{\text{in}}} = 2\pi\int_0^\infty r\,dr\int_{-\infty}^{\infty} I(r,l,t)\,dt/I_p\pi^{3/2}d^2\tau = 2\frac{\alpha e^{-\alpha l}(1-R)}{\pi^{1/2}\beta I_p(1-e^{-\alpha l})}\int_0^\infty \ln\left(1+\frac{\beta}{\alpha}I_p(1-R) \times (1-e^{-\alpha l})e^{-x^2}\right)dx. \quad (10)$$

At low intensity, we find

$$\lim_{I_p\to 0} T = (1-R)^2, \quad (11)$$

$$\lim_{I_p\to 0} d\left(\frac{1}{T}\right)\Big/dI_p = \beta l/[2^{3/2}(1-R)]. \quad (12)$$

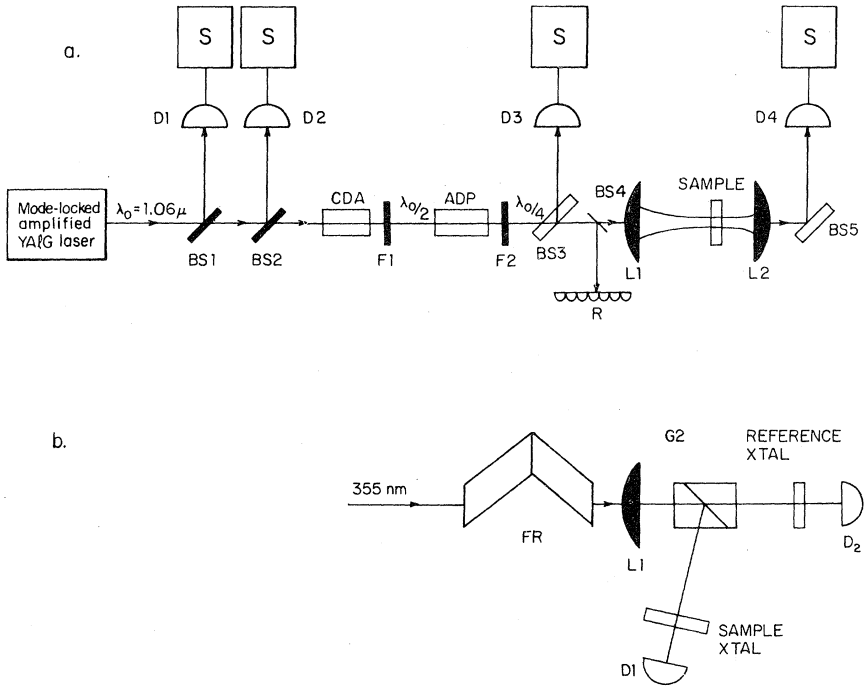

FIG. 1. (a) Schematic diagram of the absolute TPA experimental setup at 266 nm. BS: Fused silica beam splitters; D: vacuum photodiodes; L: quartz lenses; F: color filters (Corning Glass 1-56, 7-54); R: linear photodiode array; S: scope or electronic integrator. (b) Schematic diagram of the relative measurement setup. G: Glan prisms, FR: double Fresnel rhomb, L: lens, D: photodiodes.

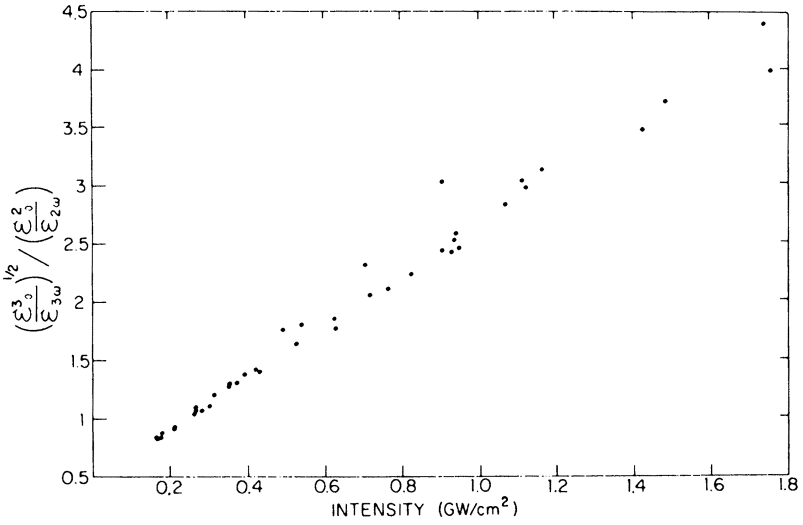

FIG. 2. Ratio of τA, found by using the third- and second-harmonic beams, plotted as a function of the fundamental input intensity. The input intensity is corrected using $(\tau A)_2$ obtained by the second-harmonic beam.

The approximation is good for $I_p(1-R)(1-e^{-\alpha l})\beta/\alpha < 1$ and $\alpha \ll 1$, which is satisfied in all samples. Thus, the slope of $1/T$ vs I_p at low intensities will give the TPA coefficient. During the TPA measurement a planar vacuum photodiode D_1 is used with a fast oscilloscope to make sure that the beam is a single pulse. The fluctuation in the pulse area and duration is taken into account by monitoring the energies of each pulse at 1.06 μm and its harmonics.[20] A fundamental Gaussian pulse

$$I_0(r,t) = I_p \exp[-(r/d)^2 - (t/\tau)^2] , \tag{13}$$

generates a second harmonic

$$I_{2\omega}(r,t) = g_{2\omega} I_p^2 \exp[-2(r/d)^2 - 2(t/\tau)^2] .$$

Here $g_{2\omega}$ is the conversion efficiency. The energy of the fundamental is $\mathcal{E}_0 = \pi^{1/2} I_p \tau A$, where $A = \pi d^2$. The second-harmonic energy is $\mathcal{E}_{2\omega} = g_{2\omega} \pi^{1/2} I_p^2 (\tau A)_2$, where $(\tau A)_2 = 2^{-3/2} \tau A$. Similarly, the third and fourth harmonics have $\mathcal{E}_{3\omega} = g_{3\omega} \pi^{1/2} I_p^3 (\tau A)_3$, $\mathcal{E}_{4\omega} = g_{4\omega} \pi^{1/2} I_p^4 (\tau A)_4$, with $(\tau A)_3 = 3^{-3/2} \tau A$, $(\tau A)_4 = 8^{-1} \tau A$. For constant conversion efficiency, we may write

$$\mathcal{E}_0^2/\mathcal{E}_{2\omega} \propto (\mathcal{E}_0^3/\mathcal{E}_{3\omega})^{1/2} \propto (\mathcal{E}_0^4/\mathcal{E}_{4\omega})^{1/3} \propto \tau A . \tag{14}$$

However, as is shown in Fig. 2, the experimental ratio of $(\mathcal{E}_0^3/\mathcal{E}_{3\omega})^{1/2}/(\mathcal{E}_0^2/\mathcal{E}_{2\omega})$ depends somewhat on the input intensity. This deviation from a horizontal line indicates that some saturation effects in the harmonics conversion efficiency and/or a change in the laser pulse shape occurs as the laser intensity is enhanced by increasing the voltage on the laser amplifiers. For a constant voltage, however, the ratio $(\mathcal{E}_0^3/\mathcal{E}_{3\omega})^{1/2}/(\mathcal{E}_0^2/\mathcal{E}_{2\omega})$ is nearly constant while the intensity is varied with attenuators. The latter effect and the narrowly distributed data shown in Fig. 2 show that the main fluctuation is coming from the fundamental beam and that τA technique provides a good correction from pulse to pulse at the same nominal intensity. In Fig. 3 we show a set of data plotted with and without a correction by the τA technique. This data clearly demonstrate the above statement.

The τA correction technique may introduce systematic error at high amplifier voltage setting due to saturation. In the intensity range of the TPA experiment performed here, we observed that the average τA increases by 50% at the peak power used (100 MW) using $(\tau A)_2$ obtained from the beam at 2ω for intensity corrections. We note that the harmonic signals used for obtaining the

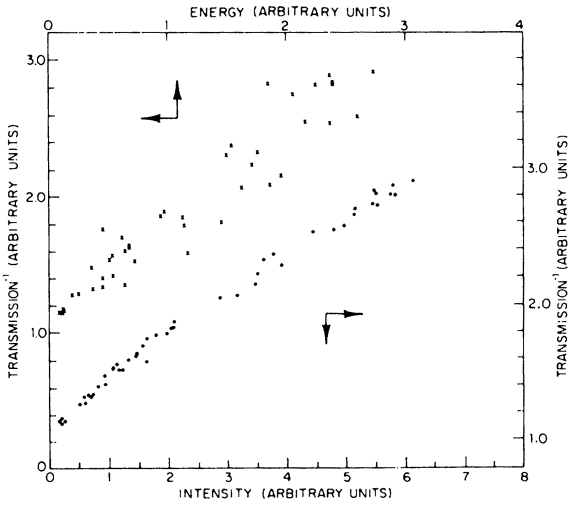

FIG. 3. Reciprocal energy transmission coefficient vs intensity (dots, analyzed with τA technique) or energy (crosses, analyzed without τA). Note the two sets of scales.

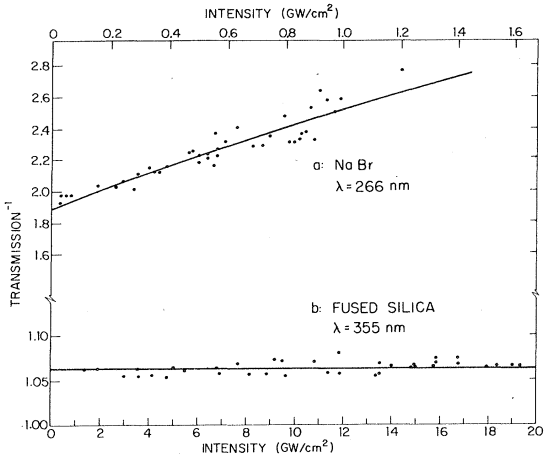

FIG. 4. (a) Plot of the reciprocal energy transmission vs maximum incident intensity for NaBr. Sample thickness is 0.74 cm, laser electric field is in the [100] direction. The drawn theoretical line is generated using Eq. (10) with $\beta = 2.5 \times 10^{-3}$ cm/MW. (b) Typical plot of inverse energy transmission vs the input intensity for materials with band gap greater than $2\hbar\omega$. Note the differences in the horizontal and vertical scales in parts (a) and (b).

various τA were obtained from the same harmonic beams utilized in the TPA experiments. The generation of 3ω, which is done in an angle tuned crystal, critically depends on the preceding second-harmonic generation step which is done in a 90° CDA crystal. Because of the nature of the mixing process, it is clear that the value of τA obtained from the energy of the beam at 2ω is more reliable than the value obtained from the beam at 3ω. Therefore, we analyzed our data using $(\tau A)_2$ for the correction.

The laser energy is measured with the diode D_3 which is calibrated with respect to a thermopile and a pyroelectric energy meter. The outputs of all photodiodes were recorded by oscillograms or by homemade peak detect-amplifier-holding circuits[21] which give the reading on digital displays. For analyzing the TPA experimental data, the approximate value of β is found using Eq. (12) and then a set of curves are generated using Eq. (10) with different values of β close to the approximate value. The TPA coefficient β is then chosen by the best fit curve as represented by the line in Fig. 4(a).

Because the TPA cross sections are rather small, a lens [see Fig. 1(a)] is used to increase the effective nonlinear absorption by increasing the intensity of the beam at the sample. Since the geometry is critical in the determination of β, the focal length of this lens ($L1$) is measured carefully. This is done at each wavelength used because the dispersion is quite large in the spectral region of the measurement.

The samples are put behind the focal point of the lens ($L1$) to avoid damage caused by the effect of self-focusing. Reflections from the back surface of the beam splitter BS3 [Fig. 1(a)] and the front surface of BS5 are used to avoid error introduced by TPA in the beam splitters themselves.

In order to eliminate any possible accumulated effects on the TPA measurement (such as F-center generation), each transmission data point was performed at a fresh site in the sample. This was done by translating the sample after each laser shot.

The circularly polarized beam used to probe the anisotropy of $\chi^{(3)}$ is generated by passing the beam through a Fresnel rhomb, with proper beam polarization. The circularity is checked by a Glan prism analyzer.

The uncertainty of the relative value of β measured here is quite small. The main contribution to this uncertainty is the uncertainty in the experimental value of τA. On the average this introduces an uncertainty of ±15%. The scattering of the data points gives on the average another ±10%. The individual uncertainty for each sample is listed in Tables I and II. The systematic error in the absolute determination of β, an uncertainty which should be added to the previous one, is ±7% in absolute energy calibration, ±28% in the average value of τA at low intensity, and ±8% caused by the ±1.5-mm uncertainty in the determination of the focal length of the lens ($L1$). Thus, the absolute uncertainty sums up to ±43%.

The experimental setup for the relative measurement with the two-channel normalization technique[6] is shown in Fig. 1(b). A double Fresnel rhomb is used here to vary in an efficient way the intensities going to the sample and reference channels. The ratio of the energy transmitted through the sample and the reference is given by

$$\rho = \frac{\mathcal{E}_s}{\mathcal{E}_r} = \frac{\alpha_s e^{-\alpha_s l_s}(1-R_s)}{1-e^{-\alpha_s l_s}} \frac{1-e^{-\alpha_r l_r}}{\alpha_r e^{-\alpha_r l_r}(1-R_r)} \frac{\beta_r}{\beta_s} \int_0^\infty \ln\left(1+\frac{\beta_s}{\alpha_s} I_s (1-R_s)(1-e^{-\alpha_s l_s}) e^{-x^2}\right) dx$$

$$\times \left[\int_0^\infty \ln\left(1+\frac{\beta_r}{\alpha_r} I_r (1-R_r)(1-e^{-\alpha_r l_r}) e^{-x^2}\right) dx\right]^{-1}. \tag{15}$$

TABLE I. TPA experimental results at 355 nm.

Material	E_g(eV) [a]	Surface normal $\vec{N}$ [b]	$\vec{E}/\lvert\vec{E}\rvert$ [c]	P_{cr}(kW) [a]	l(cm)	β(cm/MW) [d]	n [a]
KI	5.06	[100]	[001]	11	0.47	$7.29\times10^{-3}\pm20\%$	1.765
RbBr	5.40	[100]	[001]		1.0	$2.43\times10^{-3}\pm20\%$	1.600
RbI	5.04	[100]	[001]		1.0	$5.08\times10^{-3}\pm15\%$	1.731
RbI	5.04	[100]	[011]		1.0	$5.08\times10^{-3}\pm25\%$	
RbI	5.04	[100]	Circularly polarized		1.0	$4.62\times10^{-3}\pm20\%$	
ADA [e]		45° z cut	z axis		1.6	$3.53\times10^{-5}\pm30\%$	
ADP	6.81	45° z cut	z axis		2.0	$6.8\times10^{-6}\pm35\%$	1.548 (n_0) 1.499 (n_e)
Deuterated CDA		45° z cut	$\perp z$ axis		1.4	$8.02\times10^{-5}\pm30\%$	1.60 (n_0) 1.57 (n_e)
Deuterated CDA		45° z cut	z axis		1.4	$5.12\times10^{-5}\pm30\%$	1.59 (n_0) 1.57 (n_e)
CDA		45° z cut	z axis		1.15	$2.81\times10^{-5}\pm35\%$	
KDA [f]		45° z cut	z axis		1.0	$4.84\times10^{-5}\pm30\%$	1.59 (n_0) 1.54 (n_e)
Deuterated KDA		45° z cut	z axis		1.0	$2.66\times10^{-5}\pm35\%$	
KDP	6.95	45° z cut	z axis		1.0	$5.9\times10^{-6}\pm35\%$	1.531 (n_0) 1.486 (n_e)
Deuterated KDP		45° z cut	z axis		1.0	$5.4\times10^{-6}\pm35\%$	1.53 (n_0) 1.49 (n_e)
RDA [g]		45° z cut	z axis		1.25	$4.99\times10^{-5}\pm30\%$	1.60 (n_0) 1.55 (n_e)
RDP [h]		45° z cut	z axis		1.0	5.9×10^{-6}	1.53 (n_0) 1.50 (n_e)
A_2O_3	7.3	C axis			0.5	$<1.6\times10^{-6}$	1.796 (n_0)
SiO_2 (fused silica)	7.8				0.64	$<1.25\times10^{-6}$	1.476

[a] Energy band gap E_g, self-focusing critical power P_{cr}, and refractive index n are given whenever available.
[b] All measurements were done normal to the crystal surface.
[c] $\vec{E}/\lvert\vec{E}\rvert$ is the direction of the laser polarization.
[d] The total uncertainty in β is the sum of the relative uncertainty (listed in the table for each material) and the systematic uncertainty of the experiment estimated to be ±43%.
[e] ADA: ammonium dihydrogen arsenate.
[f] KDA: potassium dihydrogen arsenate.
[g] RDA: rubidium dihydrogen arsenate.
[h] RDP: rubidium dihydrogen phosphate.

TABLE II. TPA experimental results at 266 nm.

Material	E_g(eV) [a]	Surface normal $\vec{N}$ [b]	$\vec{E}/\lvert\vec{E}\rvert$ [c]	P_{cr}(kW) [a]	l(cm)	β(cm/MW) [d]	m^*/m [e]	n [a]
NaCl	6.36	[100]	[001]	16	0.74	$3.5 \times 10^{-3} \pm 25\%$	5.3×10^{-3}	1.637
NaCl	6.36	[100]	[011]	16	0.74	$3.6 \times 10^{-3} \pm 30\%$		
NaBr	7.7	[100]	[001]	8	0.74	$2.5 \times 10^{-3} \pm 15\%$	1.03×10^{-2}	1.803
KCl	6.52	[100]	[001]	20	0.74	$1.7 \times 10^{-3} \pm 20\%$	2.46×10^{-2}	1.571
KCl (F centers)		[100]	[001]	20	0.74	$1.8 \times 10^{-3} \pm 30\%$		
KCl	6.52	[100]	[001]	20	2.10	$2.7 \times 10^{-3} \pm 30\%$		
KBr	6.00	[100]	[001]	4.5	0.74	$2.0 \times 10^{-3} \pm 30\%$	1.46×10^{-2}	1.76
KI	5.06	[100]	[001]	6	0.47	$3.75 \times 10^{-3} \pm 30\%$	4.8×10^{-3}	1.938
RbCl	7.29	[100]	[001]		0.60	$1.02 \times 10^{-3} \pm 15\%$	4.54×10^{-2}	1.576
RbCl	7.29	[100]	[001]		1.91	$1.26 \times 10^{-3} \pm 30\%$		
RbBr	5.40	[100]	[001]		1.0	$2.18 \times 10^{-3} \pm 20\%$	2.02×10^{-2}	1.686
RbI	5.04	[100]	[001]		1.0	$2.49 \times 10^{-3} \pm 20\%$	1.15×10^{-2}	1.917
$CaCO_3$	5.88				0.43	$2.4 \times 10^{-4} \pm 30\%$	1.11	1.750 (n_0) 1.526 (n_e)
KDP	6.95	1.06 $\mu \rightarrow$ 0.53 μ cut		67	0.57	$2.7 \times 10^{-4} \pm 30\%$	0.72	1.560 (n_0) 1.510 (n_e)
ADP	6.81				0.5	$2.4 \times 10^{-4} \pm 30\%$	0.90	1.580 (n_0) 1.527 (n_e)
Al_2O_3	7.3	C axis			0.5	$2.7 \times 10^{-4} \pm 30\%$	0.353	1.833 (n_0)
Al_2O_3	7.3	$\perp C$ axis			0.5	$2.7 \times 10^{-4} \pm 30\%$		
SiO_2 (fused silica)	7.8			70	0.64	4.5×10^{-5}	50	
SiO_2 (Quartz)	7.8	C axis			1.2	4.5×10^{-5}	50	
LiF	11.6	[100]	[001]	73	0.47	$<2 \times 10^{-5}$		1.415
CaF_2	10.0	[100]	[001]	60	0.47	$<2 \times 10^{-5}$		

[a] Energy band gap E_g, self-focusing critical power P_{cr}, and refractive index n are given whenever available.

[b] All measurements were done normal to the crystal surface.

[c] $\vec{E}/\lvert\vec{E}\rvert$ is the direction of the laser polarization.

[d] The total uncertainty in β is the sum of the relative uncertainty (listed in the table for each material) and the systematic uncertainty of the experiment estimated to be ±43%.

[e] m^*/m is the ratio of the effective mass fitted with the Keldysh formula to the observed value of β and the mass of the free electron.

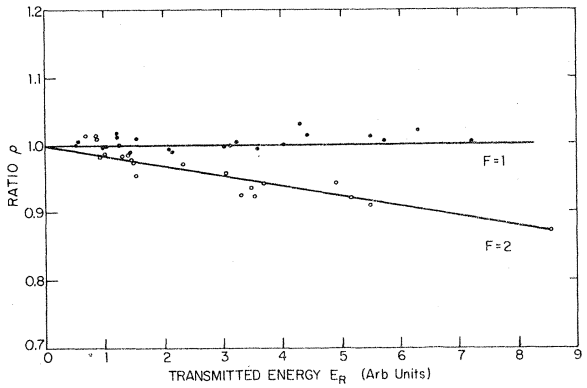

FIG. 5. Ratio of energy transmitted through the sample and the reference vs the energy transmitted through the reference in the relative measurement. Data were taken with KI vs KI with different filter factors $F=1$ (dots), $F=2$ (circles).

At proper filter factor $F = I_s/I_r$, the integrands in Eq. (15) are equal and the ratio ρ will be independent of intensity. We have then

$$\beta_s/\beta_r = \alpha_s(1-R_r)(1-e^{-\alpha_r l_r})/F\alpha_r(1-R_s)(1-e^{-\alpha_s l_s}). \tag{16}$$

To check the reliability of the setup for this experiment we used identical samples of KI as sample and reference. Figure 5 shows clearly that the expected value of $F=1$ was obtained.

IV. EXPERIMENTAL RESULTS

At 355 nm, we measured the absolute TPA coefficients in three alkali halides, as well as in KDP and 10 other harmonic-generating crystals. These are all listed in Table I. Upper limits for β in the commonly used uv window materials, sapphire and fused silica, with band gaps greater than $2\hbar\omega$ (7.02 eV) are also tabulated. For the materials measured with band gaps greater than $2\hbar\omega$, the transmission T is practically constant to intensity up to 20 GW/cm^2. Figure 4(b) shows a typical transmission plot for material with large band gap. Higher beam intensities could not be used due to the onset of surface damage.

The anisotropy of the TPA was measured in RbI. Linear polarized light in the [100] and [110] directions show the same value of β. According to Eqs. (6) and (7), this suggests the isotropy condition

$$2\chi''_{xxyy} + \chi''_{xyyx} = \chi''_{xxxx}. \tag{17}$$

The circularly polarized beam showed a smaller TPA. The ratio for the three elements of $\chi^{(3)}$ calculated from Eqs. (6)–(8) are $\chi''_{xxxx}:\chi''_{xxyy}:\chi''_{xyyx}$ = 1:0.455:0.09, with the absolute value χ''_{xxxx} = 2.72×10^{-13}cm^3/erg. Anisotropy of the tetragonal crystal deuterated CDA was also observed. The value of β with the beam polarized in the x-y plane is larger, by a factor of 1.8, than that obtained when the E field is parallel to z axis. Although some second-harmonic generation may occur in the former case, this radiation is not phase matched. The power-conversion efficiency at an input intensity of 10 GW/cm^2 is estimated to be 10^{-5} and therefore the measured value of β is not affected.

In addition to the absolute determination of β, we measured the relative values of β in RbBr vs KI and RbI vs KI as described above. The ratios obtained $\beta(\text{RbBr})/\beta(\text{KL}) = 0.305$ and $\beta(\text{RbI})/\beta(\text{KI}) = 0.668$ agree within 10% with the absolute values in Table I. This agreement between the two measurements suggests that the uncertainty estimation presented in Sec. III is quite conservative.

At 266 nm, we measured the TPA in eight alkali halides with band gap less than $2\hbar\omega$ (9.36 eV), and in KDP, ADP, calcite, sapphire, and SiO_2. The window materials LiF and CaF_2 in which no TPA is expected are also measured. The measured values are listed in Table II. For alkali halides the β values measured are of the order of 10^{-3} cm/MW, while for KDP, ADP, calcite, and sapphire, they are of the order of 10^{-4} cm/MW. For the materials with band gaps greater than $2\hbar\omega$, an upper limit for β is given. It is important to note that fused silica and quartz have quite small TPA at this wavelength.

Fluorescence is observed in all the alkali halides along the path of the beam.[22,23] Coloring can be seen with the bare eye after a few shots. In KCl the absorption of a monitoring beam at 532 nm by the color track is observed and can be explained by the spectral position of the absorption band of the F center.[24] The physical process involves the generation of electron-hole pairs by two photon excitation. The pairs recombine to form excitons with the emission of fluorescent light. The exciton energy is given up to form V_K and F centers.[25] We have found that the F centers, generated by several hundred shots of the laser at the same site of the crystal, did not influence the transmission of the crystal at the laser frequency after they had relaxed in few seconds.

Since the power used in the TPA experiment is much higher than the critical power for self-focusing,[12,26] it is important to look for any change in beam size due to self-focusing. The checks have been done with different sample thickness, also by observing the stable color track formed in a U-center-doped KCl under microscope. An attempt was made to record a single-shot beam profile in three dimensions by the TPA-generated color cen-

ters in KCl,[27] but the coloring effect is not strong enough to be observed after a single shot. No evidence of self-focusing has been observed, as discussed further in Appendix B.

Our values of β are about a factor of 5 smaller than those obtained more than a decade ago by Fröhlich and Park.[28,29] With the less-well-controlled beams, nominal values for the intensity are probably considerably lower than the actual intensity in hot spots due to spatial and temporal fluctuations. This could explain their systematically high value of β. A more recent measurement of TPA coefficient $\beta = 2.36 \times 10^{-3}$ cm/MW, by Mollenauer *et al.*,[27] in KCl is more in line with our data. Reintjes[30] has very recently reported very low values of the TPA coefficients in ADP and deuterated KDP. His value for deuterated KDP $\beta = (2.7 \pm 0.7) \times 10^{-5}$ cm/MW is an order of magnitude lower than our value for the undeuterated KDP. His value for ADP $\beta = (1.1 \pm 0.3) \times 10^{-4}$ cm/MW is a factor of 2.2 lower than ours. The large deviation of the results in the two latter crystals may be explained by differences in impurity concentration in the sample used. It is interesting to note that for the alkali halides, we measured at both uv frequencies, the TPA coefficients at 355 nm are of the same order but somewhat larger than those at 266 nm.

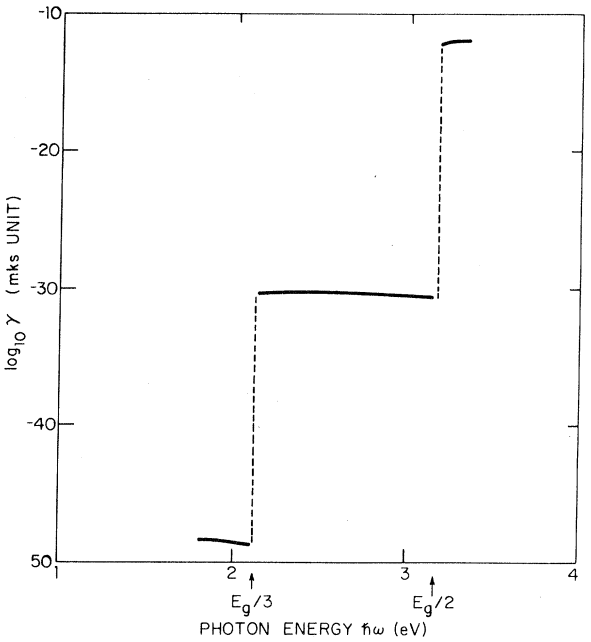

FIG. 6. Log_{10} of the multiphoton absorption coefficients in NaCl as given by the Keldysh formula vs photon energy ($m^*/m = 1$ was used). The steps indicate transitions from four- to three- and to two-photon process. The arrows indicate the photon energy as fraction of the energy band gap E_g.

V. COMPARISON WITH THE KELDYSH THEORY

The magnitudes for four-photon, three-photon, and two-photon absorption coefficients of NaCl derived from the Keldysh theory [Eq. (4)] are plotted as a function of photon energy in Fig. 6. For a fixed N, γ_N goes through a very shallow maximum as a function of photon energy. The maximum occurs at an energy just before the next lower-order photon process becomes possible. The band-gap dependence and the effective-mass dependence of γ_2, which represent the material dependence in the Keldysh theory, are shown in Fig. 7.

The observed values of β in Table II with the known band gap for each material can all be fitted with the Keldysh theory, by adjusting m^* in each case. These adjusted values of m^* are listed in Table II. It should not be expected that these values correspond to those determined by transport properties from carriers near the bottom of the conduction band. In fact, m^* in the Keldysh theory is largely a measure for the average strength of the dipole matrix element.

Using the m^* found at 266 nm for KI, RbBr, and RbI, the frequency dependence of β in each of these materials was calculated. The results are plotted in Fig. 8, along with the experimental points. It is interesting to see that the Keldysh theory does predict a decrease of β with increasing photon energy in qualitative agreement with the experimental trend.

The effect of multiphoton absorption on breakdown can also be calculated by the Keldysh formula. In order to compare this model with the experimental data observed by Smith *et al.*,[12,31] we

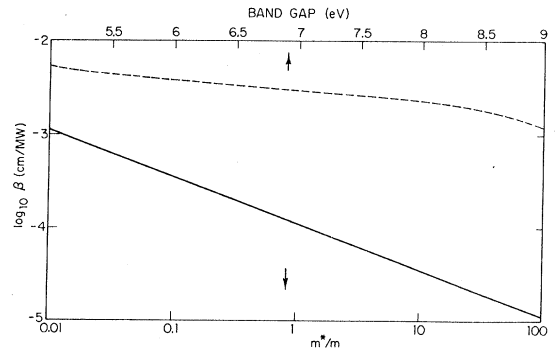

FIG. 7. Theoretical value of β vs the effective mass (dashed curve) and vs the band gap (continuous line). The parameters used in the calculation are $m^*/m = 5.3 \times 10^{-3}$ in the upper curve and $E_g = 6.36$ eV in the lower curve.

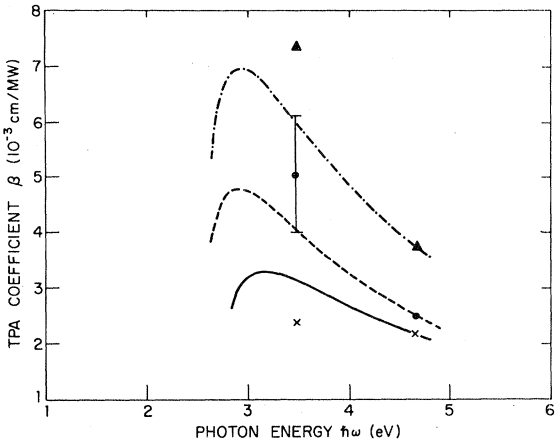

FIG. 8. Input-photon energy dependence of β. The experimental results are shown by ▲ for KI, × for RbBr, and ● for RbI. The error bar represents only the relative uncertainty. Theoretical dispersion curves are calculated by Eq. (4) using the values of the effective mass found at 266 nm.

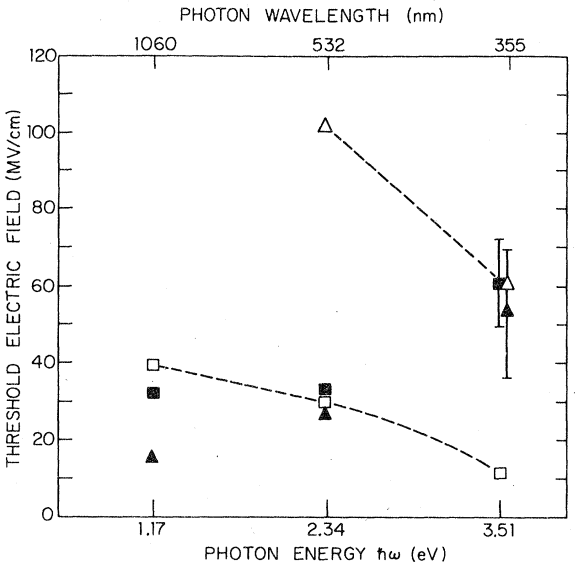

FIG. 9. Theoretical calculation according to Eq. (17) (open points) and experimental data (filled points) of the threshold peak electric field for breakdown in KDP (squares) and fused silica (triangles). The dashed curves are used to aid in reading the figure. The breakdown in silica is apparently determined by avalanche ionization, and not by multiphoton absorption.

calculated the threshold electric field needed to generate enough free electrons by multiphoton absorption alone, and melt the sample by plasma heating. Assuming no recombinations during a square picosecond laser pulse, the temperature rise by the free-electron absorption is given by

$$\Delta T = (e^2\tau/4mc)WE^2(\Delta t)^2[1/(1+\omega^2\tau^2)]\,. \qquad (18)$$

Here c is the specific heat, m is the free-electron mass, τ is the momentum-transfer collision time, Δt is the pulse duration, E is the peak electric field strength, ω is the angular frequency of the light, and W is given by the Keldysh formula [Eq. (3)]. Using Eq. (18) with m^* obtained from the theoretical fit of the TPA measurements at 266 nm and a relaxation time $\tau = 5\times10^{-16}$sec,[12] the electric field threshold for breakdown is calculated. The results for KDP and fused silica are presented along with the available experimental data in Fig. 9.

As discussed in Ref. 12, the breakdown threshold at low frequency is determined by an avalanche multiplication process. In this case, a monotonic increase in the breakdown threshold is expected with increasing laser frequency. This is reflected by the experimental data on fused silica, but the contribution to the breakdown from the three-photon absorption process at the highest frequency is appreciable.

In KDP the measured breakdown thresholds at 1.06 μm and 532 nm are almost equal. An increase by a factor of 2 occurs at 355 nm. The Keldysh theory gives breakdown threshold values close to the experimental data at 1.06 μm and 532 nm. In this region the relative contributions of the avalanche ionization and the multiphoton process to the carriers generation have to be considered as discussed by Bräunlich *et al.*[32] The larger experimental threshold observed at 355 nm might reflect the nonlinear loss in the sample, which was not taken into account in the determination of the breakdown threshold reported in Ref. 31. For example, with TPA coefficient $\beta = 6\times10^{-6}$ cm/MW and tightly focused input beam with intensity $I = 2\times10^{12}$ W/cm^2, the percentage loss per 100 μm is as high as 12%. Therefore, nonlinear losses which are not negligible at the high laser intensity used should be carefully considered. In fused silica, the expected nonlinear loss at 355 nm (three-photon absorption) is quite small. Therefore, the threshold measured is reliable.

For materials in which the damage threshold is determined mainly by the avalanche mechanism, the multiphoton absorption before the focal region where breakdown would eventually occur, is an advantage. It lowers the laser intensity at hot spots in the beam, and therefore, the possibility of self-focusing and damage is reduced.

In conclusion, we have measured the absolute TPA coefficients of several commonly used uv materials and harmonic-generating crystals[33,34] at two frequencies. The frequency dependence is adequately described by the Keldysh theory. TPA has no appreciable effect on the conversion effi-

ciency in KDP and its isomorphs. We concur in this conclusion reached by Reintjes *et al.*[14]

ACKNOWLEDGMENTS

We express our indebtedness to S. Maurici for his preparation of samples, and to Dr. L. F. Mollenauer for a *U*-center-doped sample. We also thank Dr. Cid B. de Araujo for sharing equipment and useful discussions, and Richard Yen for assistance with the measurement. This work was supported by the Advanced Research Project Agency (F-44620-75-C-0088) and by NASA (NGL-22-007-117).

APPENDIX A

The relations between the TPA coefficient in different polarization conditions and the corresponding components of $\chi^{(3)}(-\omega,\omega,\omega,-\omega)$ are obtained by defining the third-order nonlinear polarization. In cubic materials only four components of $\chi^{(3)}$ are independent. By using the general permutation rules for $\chi^{(3)}$ and the additional symmetry because we are dealing with only a single laser frequency, we get for the following three cases: (i) the electric field parallel to the crystal x axis with amplitude E_0,

$$\vec{P}^{NL}(\omega)=\begin{bmatrix}3\chi^{(3)}_{xxxx}E_x^2E_x^*\\0\\0\end{bmatrix}, \tag{A1}$$

(ii) the electric field in the [110] direction with same amplitude E_0,

$$\vec{P}^{NL}(\omega)=\begin{bmatrix}3\chi^{(3)}_{xxxx}E_x^2E_x^*+6\chi^{(3)}_{xxyy}E_yE_xE_y^*+3\chi^{(3)}_{xyyx}E_y^2E_x^*\\3\chi^{(3)}_{xxxx}E_y^2E_y^*+6\chi^{(3)}_{xxyy}E_xE_yE_x^*+3\chi^{(3)}_{xyyx}E_x^2E_y^*\\0\end{bmatrix}, \tag{A2}$$

(iii) the electric field is circularly polarized, $\vec{E}=E_0(\hat{x}+i\hat{y})$,

$$\vec{P}^{NL}(\omega)=\begin{bmatrix}3\chi^{(3)}_{xxxx}E_x^2E_x^*+6\chi^{(3)}_{xxyy}E_yE_xE_y^*-3\chi^{(3)}_{xyyx}E_y^2E_x^*\\3i\chi^{(3)}_{xxxx}E_y^2E_y^*+6i\chi^{(3)}_{xxyy}E_xE_yE_x^*-3i\chi^{(3)}_{xyyx}E_x^2E_y^*\\0\end{bmatrix}. \tag{A3}$$

The TPA work done on the material is given by $w=\mathrm{Re}(\frac{1}{2}\vec{P}\cdot\vec{E}^*)$. The TPA coefficient is defined by

$$\beta=w^2/I^2. \tag{A4}$$

Using the expression for the laser intensity for linearly polarized light

$$I=(n_0c/8\pi)E_0^2, \tag{A5}$$

and for circularly polarized light

$$I=(n_0c/4\pi)E_0^2, \tag{A6}$$

with the nonlinear polarizations given above, Eqs. (6)–(8) given in the text are easily obtained.

APPENDIX B

As mentioned in Sec. III, a fused silica (24.7-cm focal length at 355 nm) lens was used to increase the intensity per unit energy of our pulses in the sample, and a second lens after the sample was used to recollimate the pulses for final energy detection. The samples were always placed behind the focal point of the first lens by at least 2 cm, i.e., many Rayleigh lengths. There are two advantages to this placement.

First, since the sample positions were well into the region describable by geometrical optics, the calculation of the area of the pulses in the sample is less susceptible to error arising from lens aberration. In these experiments the pulse area was measured at the focusing lens plane by a photodiode array with 50-μm resolution. This measured area was used along with the carefully measured (±0.6%) focal length of the focusing lens to calculate, using diffraction-limited theory, the pulse area in the samples. The area at the sample plane could not be measured with the photodiode array due to insufficient resolution and susceptibility to damage of the detector array.

Second, the placement of the samples far beyond the lens focal point has an advantage for the reduction of harmful self-focusing effects in the experiment. If a high-power experiment is conducted in a medium at, or within a Rayleigh length of, the

focal point of a lens, then strict attention must be given to whole-beam self-focusing.[12] The input power must be kept well below the self-focusing critical power for each material in order to prevent nonlinear focal area shrinkage. However, far away from a focal region and in thin samples such as were used in these experiments, a pulse with many times the critical power may be propagated through the sample without catastrophic self-focusing. In the unfocused thin sample geometry, small-scale self-focusing[35] is the phenomenon to be avoided. In a medium of length l with a nonlinear refractive index n_2, spatial profile modulation (noise) of the input beam is augmented in intensity during propagation at most by a factor e^B. The so-called B integral[35] is

$$B=\frac{(8\times 10^7)\pi^2 n_2(esu)}{\lambda}\int_0^l I(z)\,dz\,. \tag{B1}$$

Values of n_2 are obtainable from the literature[12] for several of the materials used in this study. Calculations using Eq. (B1) confirm that in these experiments it was possible, with only two exceptions, to obtain sufficient absorption and measure accurately the TPA coefficients without incurring appreciable noise enhancement and concomitant error from small-scale self-focusing (SSSF). This conclusion was verified by the measurement of the TPA coefficient in samples of the same material and orientation but different length l. The coefficients showed no variation with l greater than the experimental uncertainty (from all sources other than SSSF) in β.

In SiO_2 at 355 nm and in LiF at 266 nm, the TPA coefficients were so small that considerably higher intensity was passed through the samples in an attempt to get measureable TPA. In these two cases, noise fluctuations of the worst-case spatial frequency may have undergone intensity growth by as much as a factor e^1, or about 3. Nevertheless, TPA coefficients were not large enough to be measured in these two cases and upper bounds only were determined. The reader should note that the n_2 values employed in the above discussion were measured[12] at 1.06 μm. At the shorter wavelengths of 355 and 266 nm, the true n_2 values may be somewhat different due to positive or negative contributions due to the nearby resonant two-photon energy bands. Resolution of that question must await n_2 measurements in the uv. From this discussion and the absence of any visual evidence, it may be concluded that self-focusing effects were not important in the evaluation of our data.

---

*Present address: Lawrence Livermore Lab., Livermore, Calif. 94550.

†Present address: General Motors Research Lab., Warren, Mich. 48090.

[1]M. Goppert-Mayer, Ann. Phys. (Leipz.) 9, 273 (1931).

[2]W. Kaiser and C. G. B. Garrett, Phys. Rev. Lett. 7, 229 (1961).

[3]J. M. Worlock, in *Laser Handbook*, edited by T. Arecchi and F. Schulz-Dubois (North-Holland, Amsterdam, 1972).

[4]H. Mahr, in *Quantum Electronics*, edited by H. Rabin and C. L. Tang (Academic, New York, 1975), Vol. I.

[5]V. I. Bredikhin, M. D. Galanin, and V. N. Gorkin, Ups. Fiz. Nauk 110, 3 (1973)[Sov. Phys.-Usp. 16, 229 (1973)].

[6]H. Lotem, W. L. Smith, and J. H. Bechtel, Appl. Phys. Lett. 28, 389 (1976).

[7]H. Lotem and Cid B. de Araujo, Phys. Rev. B 16, 1711 (1977).

[8]H. Lotem and R. T. Lynch, Jr., Phys. Rev. Lett. 37, 334 (1976).

[9]N. G. Basov, A. Z. Grasyuk, I. G. Zubarev, V. A. Katulin, and O. N. Krokhin, Zh. Eksp. Teor. Fiz. 50, 551 (1966) [Sov. Phys.-JETP 23, 366 (1966)].

[10]G. C. Bjorklund, L. F. Mollenauer, and W. J. Tomlinson, Appl. Phys. Lett. 29, 116 (1976).

[11]N. Bloembergen, IEEE J. Quantum Electron. 10, 375 (1974).

[12]W. L. Smith, J. H. Bechtel, and N. Bloembergen, Phys. Rev. B 12, 706 (1975).

[13]K. Kato, Opt. Commun. 13, 361 (1975).

[14]J. Reintjes and R. C. Eckardt, Appl. Phys. Lett. 30, 91 (1977).

[15]L. V. Keldysh, Zh. Eksp. Teor. Fiz. 47, 1945 (1964) [Sov. Phys.-JETP 20, 1307 (1965)].

[16]S. S. Mitra, L. M. Narducci, R. A. Shatas, Y. F. Tsay, and A. Vaidyanathan, Appl. Opt. 14, 3038 (1975).

[17]J. H. Bechtel and W. L. Smith, Phys. Rev. B 13, 3515 (1976).

[18]C. Flytzanis, in *Quantum Electronics*, edited by H. Rabin and C. L. Tang (Academic, New York, 1975), Vol. I.

[19]P. D. Maker and T. W. Terhune, Phys. Rev. 137, A801 (1965).

[20]W. L. Smith and J. H. Bechtel, J. Appl. Phys. 47, 1065 (1976).

[21]A. L. Smirl (private communication).

[22]M. Geller, D. E. Altman, and T. A. Detemple, Appl. Phys. Lett. 11, 221 (1967).

[23]J. N. Bradford, R. T. Williams, and W. L. Faust, Phys. Rev. Lett. 35, 300 (1976).

[24]W. B. Fowler, *Physics of Color Centers*, edited by W. B. Fowler (Academic, New York, 1968).

[25]Y. Toyozawa, in *Proceedings of the Fourth International Conference on Vacuum Ultraviolet Radiation Physics*, edited by E. E. Koch *et al.* (Pergamon, Hamburg, 1974).

[26]S. A. Akhmanov, R. V. Khokhlov, and A. P. Sukhorukov, in *Laser Handbook*, edited by T. Arecchi and F. Schulz-Dubois (North-Holland, Amsterdam, 1972).

[27]L. F. Mollenauer, G. C. Bjorklund, and W. J. Tomlinson, Phys. Rev. Lett. 35, 1662 (1975).

[28]D. Fröhlich, Phys. Rev. Lett. 19, 496 (1967).

[29]K. Park, Phys. Rev. Lett. 22, 1426 (1968).

[30]J. Reintjes and R. C. Eckardt, IEEE J. Quantum Electron. 13, 791 (1977).
[31]W. L. Smith, J. H. Bechtel, and N. Bloembergen, Phys. Rev. B 15, 4039 (1977).
[32]P. Bräunlich, A. Schmid, and P. Kelly, Appl. Phys. Lett. 26, 150 (1975).
[33]Alkali halides are from the Harshaw Chemical Co., Solon, Ohio 44139. KDP and ADP used at 266 nm are from the Cleveland Crystal Inc., Cleveland, Ohio 44110. KDP and its isomorphs used at 355 nm are from the Quantum Technology Inc., Grand Island, N. Y. 14072. Fused silica is from the Amersil Inc., Hillside, N. J. 07205.
[34]Linear data, including the index of refraction and absorption coefficient of the materials, used in this experiment are taken from: *American Institute of Physics Handbook, 3rd edition*, edited by Dwight E. Gray (McGraw-Hill, New York, 1972); Landolt-Börnstein, *Zahlenwert und Funktionen aus Physik. Chemie-Astro-Geophys-Tech.* (8) (Springer-Verlag, Berlin, 1962); D. N. Nikogosyan, Kvantovaya Elektron. (Moscow) 4, 5 (1977) [Sov. J. Quantum Electron. 7, 1 (1977)]; W. L. Smith, Appl. Opt. 16, 1789 (1977).
[35]E. S. Bliss, J. T. Hunt, P. A. Renard, G. E. Sommargren, and M. J. Weaver, IEEE J. Quantum Electron. 12, 402 (1976).